VERTEBRATE ZOOLOGY

70 (3): 275–290
2020

SENCKENBERG

VIRTUAL ISSUE on Recent Advances in Chondrocranium Research | Guest Editor: Ingmar Werneburg

Connecting the chondrocranium: Biomechanics of the suspensorium in reptiles

Alec T. Wilken[1,*], Kaleb C. Sellers[1], Ian N. Cost[2], Rachel E. Rozin[1], Kevin M. Middleton[1] & Casey M. Holliday[1]

[1] Department of Pathology and Anatomical Sciences, University of Missouri, M263, Medical Sciences Building, Columbia, MO, 65212, USA — [2] Department of Biology, Albright College, 13th and Bern Streets, Reading, PA, 19612, USA — * Corresponding author; atwxb6@mail.missouri.edu

Submitted February 07, 2020.
Accepted June 8, 2020.
Published online at www.senckenberg.de/vertebrate-zoology on June 16, 2020.
Published in print Q3/2020.
Editor in charge: Ingmar Werneburg

Abstract

Gnathostomes all share the common challenge of assembling 1st pharyngeal arch elements and associated dermal bones (suspensorium) with the neurocranium into a functioning linkage system. In many tetrapods, the otic and palatobasal articulations between suspensorium and neurocranial elements form the joints integral for cranial kinesis. Among sauropsids, the otic (quadratosquamosal) joint is a key feature in this linkage system and shows considerable variability in shape, tissue-level construction and mobility among lineages of reptiles. Here we explore the biomechanics of the suspensorium and the otic joint in five disparate species of sauropsids of different kinetic capacity (two squamates, one non-avian theropod dinosaur, and two avian species). Using 3D muscle modeling, comparisons of muscle moments, joint surface areas, cross-sectional geometries, and finite element analysis, we characterize biomechanical differences in the resultants of protractor muscles, loading of otic joints, and bending properties of pterygoid bones. For the first time, we quantify and directly compare biomechanical descriptors of pterygoid morphology and 3D muscle loads among disparate sauropsids. We propose three classes of pterygoids based on shape on biomechanical loading: brace, propulsive, and torsional. The tubular pterygoids of the lizards and birds appear to experience more diverse loading regimes than the mediolaterally narrow element of the non-avian dinosaur. Our new approaches and findings shed new light on our understanding of evolution and diversity of the suspensorium in tetrapods.

Key words

Biomechanics; Cranial Kinesis; Joints; Palates; Suspensorium.

Introduction

The vertebrate skull is a composite organ made from structures that arise from diverse developmental, evolutionary, and biomechanical phenomena (Schilling & Thorogood, 2000; Hirasawa & Kuratani, 2015). Of these parts, the neurocranium is among the key skeletal elements as it serves not only as primordial (i.e., chondrocranial) protection for the brain and sensory structures, but as the cartilaginous and ultimately bony structure the jawed feeding apparatus is formed about (Bellairs & Kamal, 1981). Despite the great diversity of the head structure and function among gnathostomes (e.g., Hanken & Hall, 1993), they all share the common problem of articulating the first arch cartilages and associated bones (suspensorium) to the neurocranium (Cerny *et al.*, 2004; Schoch, 2006). Although this articulation is mediated indirectly via the hyomandibula in fishes, as this suspensorial element transitioned to form the ear ossicle (i.e., the columella) in early tetrapods, the suspensoric formed a new direct link with the neurocranium via the otic joint (Brazeau & Ahlberg, 2006; Gardner *et al.*, 2010) and palatobasal joint (e.g., Iordansky, 1989). Despite considerable variation in the construction of these

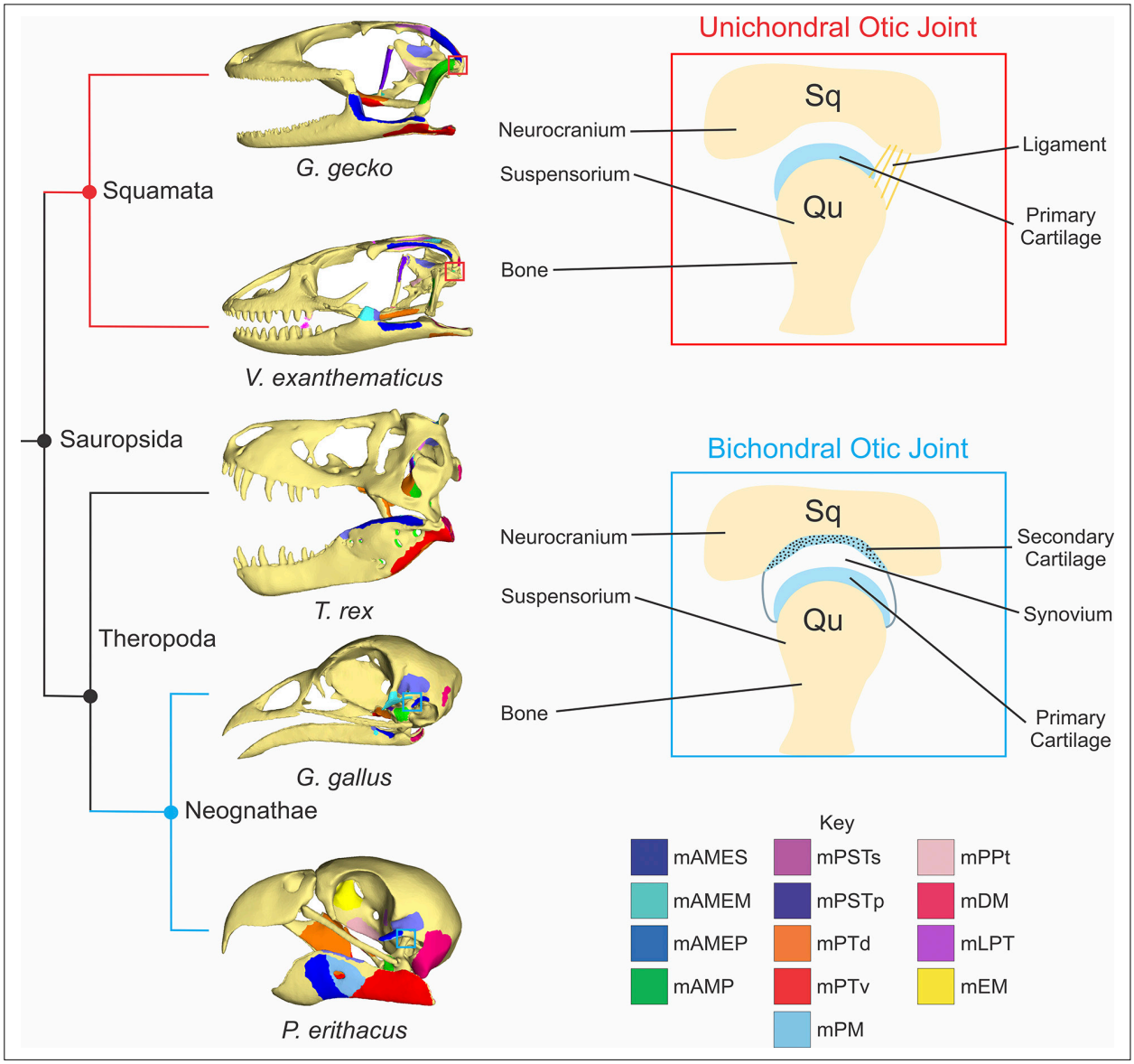

Fig. 1. Summarized variation and evolution of the otic joint. Squamates maintain a unichondral otic joint with ligamentous connections between the quadrate and neurocranium (red), while birds evolved a secondarily cartilaginous squamosal with a synovial capsule (blue). Little is known, however, about the otic joint in extinct taxa. **mAMEM,** *m. adductor mandibulae externus medialis;* **mAMEP,** *m. adductor mandibulae externus profundus;* **mAMES,** *m. adductor mandibulae externus superficialis;* **mAMP,** *m. adductor mandibulae posterior;* **mDM,** *m. depressor mandibulae;* **mEM,** *m. ethmomandibularis;* **mLPt,** *m. levator pterygoideus;* **mPM,** *m. pseudomasseter;* **mPPt,** *m. protractor pterygoideus;* **mPSTp,** *m. pseudotemporalis profundus;* **mPSTs,** *m. pseudotemporalis superficialis;* **mPTd,** *m. pterygoideus dorsalis;* **mPTv;** *m. pterygoideus ventralis*, **Qu,** quadrate, **Sq,** squamosal.

joints, they all share the function of linking the jaws to the neurocranium.

This developmentally-necessary linkage system often permits cranial kinesis (PAYNE *et al.*, 2011) in tetrapods, but the extent of this behavior in amniotes varies from sutured akinesis (i.e., immobility) in mammals, turtles, and crocodylians, to highly flexible joints in ducks, lizards, and snakes (CUNDALL, 1983; DAWSON *et al.*, 2011; MONTUELLE & WILLIAMS, 2015; WERNEBURG & MAIER, 2019), to a host of hypothesized intermediate behaviors in living and extinct species of sauropsids, such as non-avian dinosaurs and stem suchians where kinematic data are lacking (METZGER, 2002; HOLLIDAY & WITMER, 2008). To complement kinematic data, we can instead explore how these joints and bony elements mediate forces transmitted between the suspensorium and the neurocranium to better evaluate the biomechanical environment of the neurocranium (e.g., JONES *et al.*, 2017), its joints and ossified linkages, and its evolutionary history. Here we provide new approaches and findings for estimating the loading environments of the suspensoric elements and their linkages with the neurocranium in select, disparate reptile species. Historically, the anatomy of this part of the head has been challenging to understand because of its anatomical depth, complexity, and fragility (e.g., RIEPPEL, 1978; HANKEN & HALL, 1993; BOUT & ZWEERS, 2001;

Gussekloo *et al*., 2001; Evans, 2008; Holliday & Witmer, 2008). However, new imaging, biomechanical modeling, and quantitative approaches enable deeper insight into the region, its function and evolution.

Anatomically, the otic joint is built by the otic process of the quadrate, and a combination of neurocranial (e.g., prootic, exoccipital) and dermatocranial (e.g., squamosal, postorbital) elements among the various lineages of amniotes (Fig. 1). Thus, although generally similar in the position of articulation, the joints themselves are constructed in part by non-homologous elements (Holliday & Witmer, 2008). Similarly, the palatobasal joint is the linkage between the inferior portion of the ascending process of the palatoquadrate cartilage (as a part of the suspensorium; i.e. 1st arch cartilage) and the inferior neurocranium. Although the pterygoid bone and vestige of the suspensorium mediate this joint in lepidosaurs (lizards, snakes, and tuatara; Payne *et al*., *2011*; Wilken *et al*., 2019) and many dinosaurs (Holliday & Witmer, 2008), including paleognath birds (emus and ostriches; Bailleul & Holliday, 2018), the joint is formed by non-homologous portions of the palate and suspensorium in ducks (Bailleul *et al*., 2017) and perhaps other neoavian clades (extant birds excluding Paleognathae and Galloanserae). Similarly, although the epiphysis of the basipterygoid process of the basisphenoid forms the neurocranial side of the palatobasal joint in most non-dinosaurian sauropsids, portions of the parabasisphenoid likely contribute to the formation of a novel 'palatobasal' articulation during the origin of the maniraptoran and avian braincase (Holliday & Witmer, 2008). Turtles and crocodylians, however, have sutured the quadrate and pterygoid to the neurocranium thereby eliminating, or reducing, these joints to vestigial structures (e.g., Bailleul & Holliday, 2017; Werneburg & Maier, 2019).

Jaw muscles cross the otic, palatobasal, and jaw joints and act upon their attachment sites to drive movements of the jaws. Although the mandibular adductor and pterygoideus muscles are the primary drivers of closing the mandibles (Holliday & Witmer, 2007), the protractor pterygoideus musculature are responsible for mediating loads and movements between the suspensorium and the neurocranium (Wilken *et al*., 2019). Although the pterygoideus muscles and the protractor muscles are the two groups of muscles that act directly upon the palatal elements, of course we recognize the actions of the temporal and depressor mandibulae muscles also indirectly load these elements during feeding.

Histologically, the otic joint varies in composition based on the developmental origins and ossification processes that build the joint. Primitively, lizards maintain a unichondral articulation at the otic joint where the epiphyseal cartilage of the endochondrally-ossifying otic process joins with a series of ligaments from the squamosal, parietal, and exoccipital elements (Wilken *et al*., 2019). Similarly, in geckoes, the otic condyle of the quadrate is capped in hyaline cartilage that grades into fibrocartilage as it approaches the otooccipital; this connection is surrounded by fibrous connective tissue (Payne *et al*., 2011; Mezzasalma *et al*., 2014). Despite suturing all-the surrounding bony elements together, the otic joint of the American alligator, *Alligator mississippiensis*, still possesses the primitive, lepidosaur-like, albeit small epiphyseal cartilage on the otic process of the quadrate (Bailleul & Holliday, 2017). Unlike other extant sauropsids, extant birds form secondary cartilage on membranously-ossifying bones that can thus form bichondral joints and synovial joints (Hall, 2005; Bailleul *et al*., 2017) at joints that were historically unichondral. Regardless, both unichondral, sydesmodial otic joints, as well as bichondral, diarthrodial joints, seem equally capable of excursions during feeding behaviors, given that lizards, which maintain unichondral, sydemsmodial otic joints, and birds, which possess bichondral, diarthrodial otic joints, are both capable of streptostylic movement (Smith, 1980; Dawson *et al*., 2011; Claes *et al*., 2019). Indeed, Strait *et al*., (2005) and Wilken *et al*., (2019), have shown that differing soft tissue material properties of cranial joints does not necessarily impact the loading of a skull. However, other biomechanical simulations have demonstrated that non-bony tissues (e.g., sutures) distribute loads and increase strain (Moazen *et al*., 2009b; Curtis *et al*., 2011) and the presence of a non-bony neurocranium reduces strain in the cranium (Jones *et al*., 2017). In any case, Mezzasalma *et al*., (2014) showed that histological composition of cranial joints does not affect cranial kinetic capacity, but the morphology of these joints better reflects kinetic capacity. Thus, any potential excursion is instead likely mediated by the morphology of surrounding bones, the morphology and histological composition of their joints, as well as muscular control of jaw musculature.

Functionally, the quadrate and pterygoid act as struts between the otic and palatobasal joints which then link the neurocranium, maxillary, and mandibular units of the sauropsid skull. They also serve as sites of attachment for protractor, pterygoideus, and adductor posterior muscles (Holliday, 2009). Depending on the development and feeding behaviors employed by different sauropsids, we can expect different morphologies in these joints, the interlinking bony elements, the muscles that load them, and the forces that are transmitted through them. For example, in the prokinetic avian feeding system, the pterygoid functions as a force transmitter (Olsen & Westneat, 2016; Olsen, 2019), the protractor pterygoideus muscles are rostrocaudally oriented, and the pterygoid bone is largely loaded in axial compression (Cost *et al*., 2019). In the squamate feeding system the pterygoid functions as torsion resistor (Wilken *et al*., 2019); the protractor muscles are more transversely oriented and the pterygoid bone is bent and twisted about an axis near the palatobasal joint. The protractor muscles and pterygoideus muscles play important roles in mediating palatal movements (Bout & Zeigler, 1994; Herrel *et al*., 2000; Wilken *et al*., 2019). This diversity of pterygoid function in reptiles may manifest in the morphology and cross-sectional geometry of the pterygoid bone, which is informative on the bone's ability to resist bending and torsion (Vogel,

Table 1. Material Properties for FEA.

Gekko gecko			
Material	Young's Modulus (Pa)	Poisson's Ratio	Citation
Bone	1.365×10^{10}	0.30	RAYFIELD, 2011
Suture	1.0×10^{7}	0.30	MCLAUGHLIN *et al*., 2000
Varanus exanthematicus			
Material	Young's Modulus (MPa)	Poisson's Ratio	Citation
Bone	8800	0.40	ZAPATA *et al*., 2010
Suture	10	0.30	MCLAUGHLIN *et al*., 2000
Cartilage	6	0.49	BEAUPRE *et al*., 2000
Tyrannosaurus rex			
Material	Young's Modulus (Pa)	Poisson's Ratio	Citation
Bone	1.365×10^{10}	0.3	RAYFIELD, 2011
Suture	4.57×10^{8}	0.3	HAUT *et al*., 1992
Gallus gallus			
Material	Young's Modulus (Pa)	Poisson's Ratio	Citation
Bone	1.365×10^{10}	0.30	RAYFIELD, 2011
Cartilage	6000	0.49	BEAUPRE *et al*., 2000
Psittacus erithacus			
Material	Young's Modulus (Pa)	Poisson's Ratio	Citation
Bone	1.365×10^{10}	0.3	RAYFIELD, 2011
Suture	1×10^{7}	0.3	MCLAUGHLIN *et al*., 2000

1988) and the direction of normal mechanical loading occurring on the bone (PEARSON & LIEBERMAN, 2006; RUFF *et al*., 2006). Because the pterygoid is a central element in the streptostylic linkage system (OLSEN & WESTNEAT, 2016) and because rotation of the quadrate requires "accommodation" by the palate (EVANS, 2003) and these accommodating elements may become highly stressed during feeding (MOAZEN *et al*., 2009a), the bending properties of the pterygoid may also create spatial constraints on the linkage system and limit the degrees of freedom for quadrate movement.

Cranial kinesis is a manifestation of many morphological, histological, mechanical, and behavioral variables. Therefore, making informed predictions about structure-function relationships is challenging. Regardless, new methods are enabling us to better capture joint shape, function and performance. Thus, here we explore the diversity of form, function and performance across a small yet diverse sample sauropsids of varying kinetic behaviors. Using novel imaging and modeling approaches we quantify aspects of cranial morphology which affect kinetic behaviors and elucidate promising future avenues of research.

Materials and Methods

Materials

We sampled five individuals that we believe to be exemplar of disparate sauropsid lineages. An individual of *Varanus exanthematicus* (Squamata: Varanidae) [Ohio University Vertebrate Collections (OUVC) 10414] was micro-computed tomography (microCT) scanned (GE eXplorel locus, 45 µm cubic voxel size, Ohio University) to create a model of the *Varanus exanthematicus* skull. Individual OUVC 10414 was also dissected for jaw muscle architecture. An individual of *Gekko gecko* (Squamata: Gekkonidae) [University of Missouri Vertebrate Collection (MUVC) LI044] was scanned in a Siemens INVEON SPECT/CT (VA Biomolecular Imaging Center, 92.1 µm cubic voxel size, Columbia, MO). An individual of *Psittacus erithacus* (Psittaciformes: Psittacidae; MUVC AV042) was scanned in a Siemens INVEON SPECT/CT (VA Biomolecular Imaging Center, 63.4 µm cubic voxel size, Columbia, MO). A 1/6 scale model of *Tyrannosaurus rex* (Saurischia: Tyrannosauridae; BHI 3033) was scanned in a General Electric LightSpeed Ultra Multislice CT Scanner (625 µm cubic voxel size, 120 kV, 170 mA, OhioHealth, O'Bleness Memorial Hospital, Athens, OH; Cost et al., 2019). An individual of *Gallus gallus* (Galliformes: Phasianidae; MUVC AV003) was scanned in a Siemens INVEON SPECT/CT (VA Biomolecular Imaging Center, 92.2 µm cubic voxel size, Columbia, MO).

Methods

Bending Properties

Second moment of area of the pterygoid was analyzed for all the animals in this study. Pterygoid bodies were isolated from accessory palatine, quadrate and maxillary processes, in AVIZO v9.7 (Thermo Fisher Scientific, MA, US). CT data was then exported as tiffs to be analyzed in IMAGEJ 1.x (SCHNEIDER *et al*., 2012). Using the Slice Geometry tool in BONEJ (DOUBE *et al*., 2010), we collected the second moment (I; mm^4), which measures the efficiency of cross-sectional shape to resist bending,

Table 2. Muscle Modeling Parameters.

Gekko gecko				
Name	Fascicle Length (mm)	Pennation (°)	Muscle Volume (mm^3)	Force (N)
mAMES	13.09	25	445.25	47.08
mAMEP	11.85	0	180.69	25.75
mAMP	8.23	5	463.85	136.44
mPSTs	13.67	0	141.56	15.14
mPSTp	8.98	0	128.18	31.80
mPtd	7.92	15	93.97	28.92
mPtv	8.25	15	391.97	111.24
mLPt	8.48	5	28.23	7.81
mPPt	4.81	5	72.27	62.33
mDM	10.20	5	66.86	12.81
Varanus exanthematicus				
Name	Fascicle Length (mm)	Pennation (°)	Muscle Volume (mm^3)	Force (N)
mAMES	11.00	7	304.43	4.99
mAMEM	13.28	0	147.61	1.67
mAMEP	10.31	7	82.85	1.55
mAMP	6.11	5	154.08	8.22
mPSTs	11.39	7	210.19	3.21
mPSTp	8.38	0	23.87	0.68
mPt	6.77	19	188.92	7.79
mLPt	10.95	0	5.02	0.13
mPPt	4.21	5	29.94	2.67
mDM	8.60	5	99.34	3.37
Tyrannosaurus rex				
Name	Fascicle Length (cm)	Pennation (°)	Muscle Volume (cm^3)	Force (N)
mAMES	46	0	20,971	3,343
mAMEM	52	0	17,729	9,841
mAMEP	57	0	11,914	6,635
mAMP	28	15	37,120	39,859
mPSTs	55	10	7,792	4,209
mPSTp	41	10	2,668	1,865
mPtd	32	10	40,106	34,816
mPtv	28	15	8,562	8,820
mLPt	6	0	545	3,180
mPPt	10	15	2,187	5,489
mDM	25	5	8,981	10,206
Gallus gallus				
Name	Fascicle Length (mm)	Pennation (°)	Muscle Volume (mm^3)	Force (N)
mAMES	1.59	12.4	0.14	2.6
mAMEM	2.08	0	0.15	2.12
mAMEP	2.08	0	0.30	4.27
mAMP	2.85	0	0.15	1.53
mPSTs	4.68	16.9	0.04	0.25
mPSTp	4.68	18.9	0.02	0.13
mPtd	1.43	5	0.12	2.20
mPtv	2.03	10.75	0.10	1.28
mPPt	1.59	12.4	0.03	0.47
mDM	2.08	0	0.19	2.70
Psittacus erithacus				
Name	Fascicle Length (mm)	Pennation (°)	Muscle Volume (mm^3)	Force (N)
mAMES	15.06	20	1077.70	20.17
mAMEP	16.92	20	702.10	13.46
mAMP	2.70	0	63.34	7.05
mPSTs	13.41	6.66	266.93	6.351
mPtd	11.07	14.54	2636.37	23.118
mPtv	9.60	4.09	1541.95	48.08
mPPt	10.17	0	360.79	4.54
mEM	14.98	2.57	981.52	19.64
mPM	20.81	0	1241.92	17.91
mDM	7.00	5.52	848.32	36.21

about the major (I_{max}) and minor axis (I_{min}) for all slices. Although CT data for *T. rex* specimen FMNH PR2081 ("Sue") is available (BROCHU, 2003), these data were of too low resolution to provide adequate second moment of area data. Instead, we used slices of the FEA model from COST *et al*. (2019) with the Sue CT data informing us on the cross-sectional geometry of the *T. rex* pterygoid. To compare the data, second moment about the minor axis was divided by second moment about the major axis and these results were plotted against a percent length of the pterygoid.

Joint Surface Areas

Articular surfaces of the squamosal and quadrate were collected from each specimen using AVIZO v9 (Thermo Fisher Scientific, MA, US) and GEOMAGIC STUDIO v13 (3D Systems, NC, US) and provided surface area measurements. Each taxa had an n of 1 for this measurement; however given the broad taxonomic scope of this study we believe intraspecific variation to be negligible with respect to this study's goals. Joint surface areas were compared by dividing the quadrate articular surface by the squamosal articular surface to create a rough estimate of joint congruency. The squamate otic head of the quadrate is anatomically complicated and serves as both an articular surface for the otic joint and as an attachment site for ligamentous connections. Therefore, for the squamate taxa sampled here we only collected the surfaces which likely function as part of the otic joint.

FEA

Model Construction. CT images were segmented and analyzed in AVIZO v5.2 and v9 (Thermo Fisher Scientific, MA, US) to create three-dimensional skull models. These models were then imported into GEOMAGIC STUDIO v7, v13 (3D Systems, NC, US) where the models were cleaned for meshing, aligned to similar axes (z being rostral-caudal, y being dorsal-ventral, and x being medial-lateral, with the point (0,0,0) being in line with the jaw joint, ventral to the occipital process). Models were then imported into STRAND7 (Beaufort Analysis, Sydney, AUS) where they were meshed with four noded tetrahedra. The *Gekko gecko* model has 189,587 nodes and 789,722 tetrahedra. The *Varanus exanthematicus* model has 243,071 nodes and 1,016,754 tetrahedra. The *Tyrannosaurus rex* model has 76,948 nodes and 306,684 tetrahedra. The *Gallus gallus* model has 80,154 nodes and 322,921 tetrahedra. The *Psittacus erithacus* model has 112,015 nodes and 432,007 tetrahedra.

To better understand biomechanical interactions at particular articulations, joints were modeled using flexible beams to act as articular tissues (WILKEN *et al*., 2019); however, the fibrous components of the joint capsules were not modeled. These joints included: the palatobasal joint, otic joint, frontoparietal suture, craniofacial hinge, and articulations of the epipterygoid with the prootic and pterygoid. Material properties of these beams (Table 1) were informed by histological data; however, the material properties were not derived from these data. Instead, material properties were gleaned from existing literature (Table 1).

Muscle Modeling. For extant taxa, jaw muscles were dissected to examine fascicle orientation and length to calculate physiological cross-sectional area (PCSA; Table 2). Attachment sites for jaw muscles were determined by literature review, dissection, and DiceCT: *Gekko gecko* (new dissection and DiceCT; see COST *et al*., 2019), *Varanus exanthematicus* (new dissection, DiceCT, and HOLLIDAY, 2009; see WILKEN *et al*., 2019), *Psittacus erithacus* (new dissection, DiceCT, and GIGNAC *et al*., 2016; see COST *et al*., 2019), *Gallus gallus* (new dissection), and *T. rex* (HOLLIDAY, 2009; see COST *et al*., 2019). These methods were also used to determine fiber length and pennation angle. These attachment sites were then mapped on to the model to calculate surface area of attachment and muscle volume. *Sensu* SELLERS *et al*., (2017) muscle volume was treated as a frustum, a cone with its apex cut off parallel to its base. This volume is defined by Eqn 1 (SELLERS *et al*., 2017):

$$V_m = \frac{l_m}{3}(A_{or} + A_{ins} + (\sqrt{A_{or} + A_{ins}}) \quad (1)$$

where l_m is muscle length, A_{or} is area of muscle origin, and A_{ins} is area of muscle insertion (SELLERS *et al*., 2017). Muscle volume (V_m)can then be used to calculate PCSA with Eqn 2 (SACKS & ROY, 1982):

$$PCSA = \frac{V_m}{l_m} \cdot \cos(\theta) \quad (2)$$

where l_f is fiber length and θ is angle of pennation (SACKS & ROY, 1982). Using the BONELOAD workflow, (DAVIS *et al*., 2010; SELLERS *et al*., 2017), muscle forces were calculated from Eqn 3 (GANS, 1982):

$$F_m = PCSA \cdot T_{specific} \quad (3)$$

→ **Fig. 2.** Muscle orientations of palatal muscles. **A**, 3-D visualization of palatal muscle resultant orientations for *G. gecko* in left lateral oblique and ventral views, **B**, 3-D visualization of palatal muscle resultant orientations for *Varanus exanthematicus* in left lateral oblique and ventral views, **C**, 3-D visualization of palatal muscle resultant orientations for *Tyrannosaurus rex* in left lateral oblique and ventral views, **D**, 3-D visualization of palatal muscle resultant orientations for *Gallus gallus* in left lateral oblique and ventral views, **E**, 3-D visualization of palatal muscle resultant orientations for *Psittacus erithacus* in left lateral oblique and ventral views, **F**, ternary diagram of *m. protractor pterygoideus* orientations, **G**, ternary diagram of *m. levator pterygoideus* orientations, **H**, ternary diagram of *m. pterygoideus ventralis* orientations, and **I**, ternary diagram of *m. pterygoideus dorsalis* orientations. There is considerable variation in *m. protractor pterygoideus* resultant orientation, displaying the many biomechanical roles it likely plays in the suspensorium.

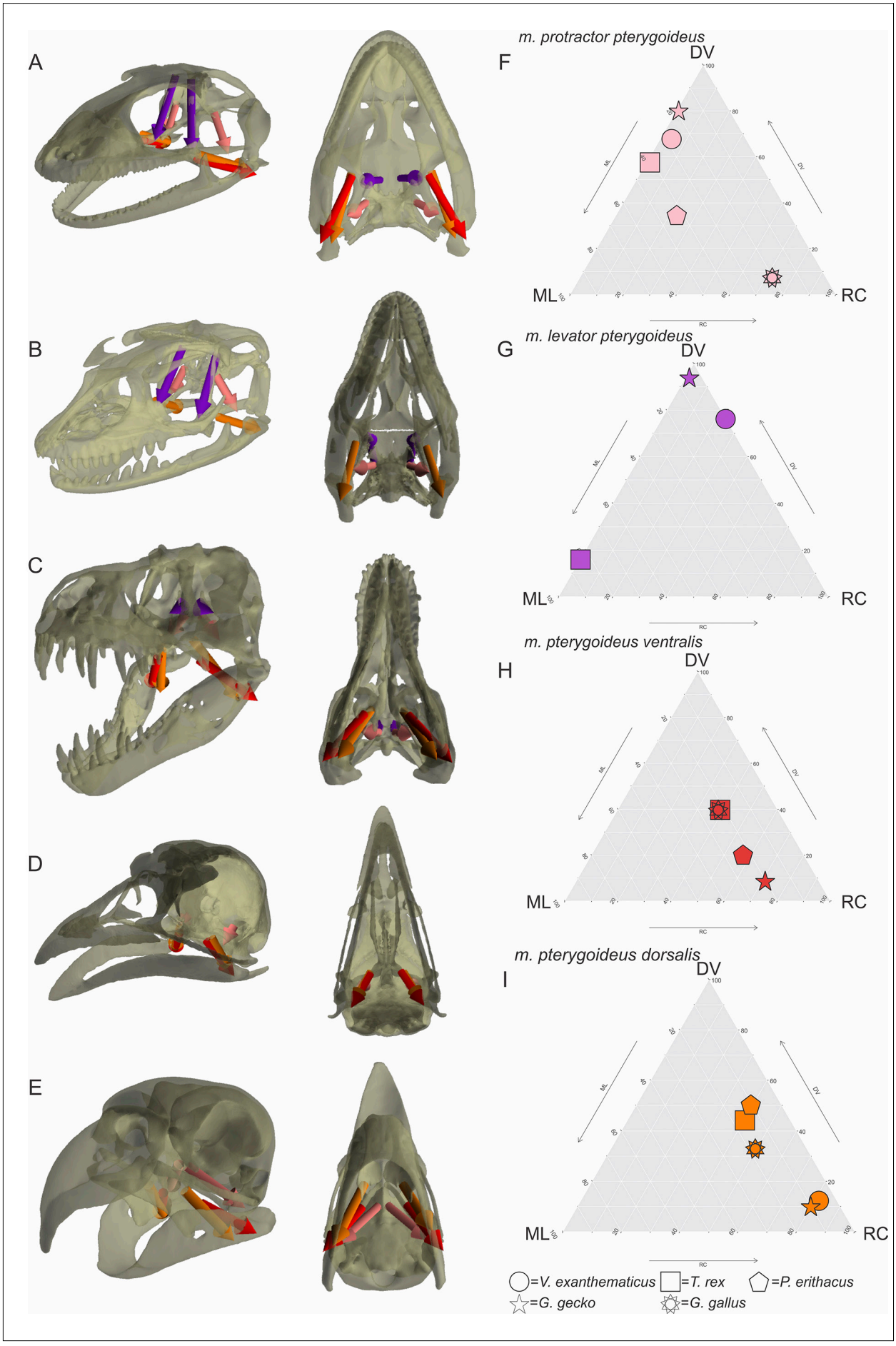
A
B
C
D
E
F
m. protractor pterygoideus
DV
ML
RC
G
m. levator pterygoideus
H
m. pterygoideus ventralis
I
m. pterygoideus dorsalis
=V. exanthematicus
=T. rex
=P. erithacus
=G. gecko
=G. gallus

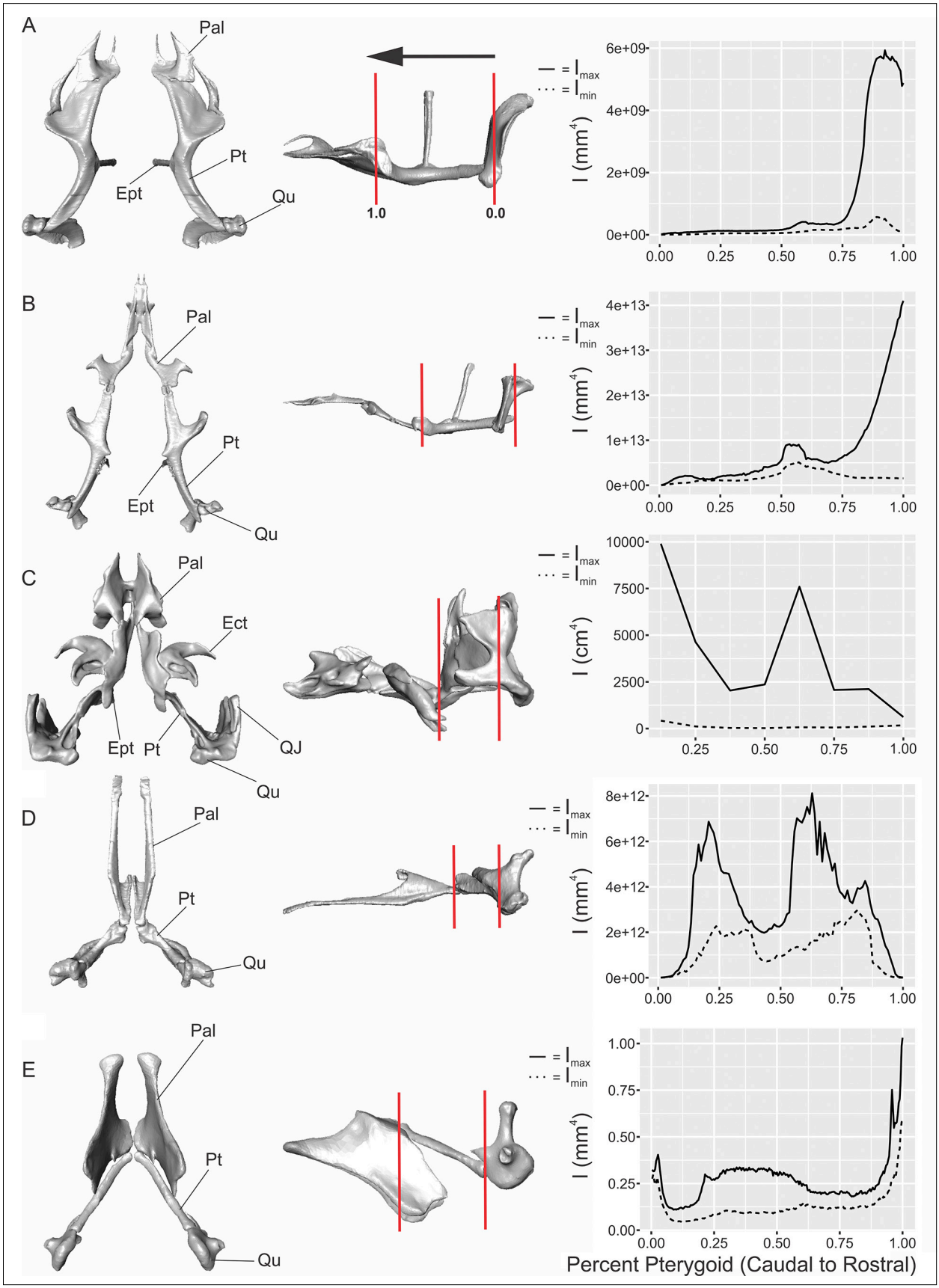

Fig. 3. Pterygoid cross-sectional geometries. A, *Gekko gecko* palate ventral and left lateral views and bending resistance, B, *Varanus exanthematicus* palate ventral and left lateral views and bending resistance, C, *Tyrannosaurus rex* palate ventral and left lateral views and bending resistance, D, *Gallus gallus* palate ventral and left lateral views and bending resistance, and E, *Psittacus erithacus* palate ventral and left lateral views and bending resistance. Bending properties illustrate which axes the pterygoid is most resistant in. Higher values of I indicate greater resistance to bending. **Ect,** ectopterygoid; **Ept,** epipterygoid; **Pal,** palatine; **Pt,** pterygoid; **QJ,** quadratojugal; **Qu,** quadrate.

where F_m is muscle force and $T_{specific}$ is the specific tension of the muscle (Gans, 1982). See Table 2 for muscle modeling data. Using Boneload, these forces were applied over the areas of jaw muscle attachment sites. *Tyrannosaurus rex* muscle modeling and force calculations are detailed in Cost *et al*., (2019). The pennation angles of *T. rex* were estimated to fall within the phylogenetic bracket of pennation angles in alligator, bird, and lizard jaw muscles; furthermore, muscles in *T. rex* were modeled to have fiber lengths that are two-thirds the length of the muscle (Cost *et al*., 2019).

***Finite Element Analysis*.** Constraints allowing 0 movement in any direction were placed on the jaw joint, the center of the paraoccipital, supraoccipital, and caudal bite point. To examine loading on the otic joint we collected principal strains from the articular surface of the quadrate and calculated the mean and variance of these principal strains. Data were collected in strain because strain is unitless and therefore more comparable between specimens of different proportions.

Ternary Plots

Using muscle attachment sites and muscle forces generated from the Boneload workflow (see above), ternary diagrams of jaw muscle resultant vector orientations (Wilken *et al*., 2019) were plotted to better visualize and compare the orientations of muscle forces. The code for this analysis can be found at https://github.com/Middleton-Lab/MuscleTernary. Because we were only interested in the orientation, not the magnitude, of the jaw muscles forces, scaling of jaw muscle force magnitude is constant in these diagrams.

Results

Muscle Orientation

We plotted comparative ternary diagrams of *m. protractor pterygoideus* (mPPt), *m. levator pterygoideus* (mLPt), *m. pterygoideus dorsalis* (mPtd), *and m. pterygoideus ventralis* (mPtv; Fig. 2), which attach to the pterygoid and play diverse roles in cranial kinesis (Bout & Zweers, 2001; Gussekloo *et al*., 2001; Holliday & Witmer, 2008; Wilken *et al*., 2019). Overall, these plots illustrate a range of possible orientations for these muscles in the reptile lineages studied here.

Gekko gecko possesses the most dorsoventral *m. protractor pterygoideus* (mPPt) orientation (Fig. 2A), while *Gallus gallus* possesses the most rostrocaudal mPPt orientation (Fig. 2D). Within this range of orientation space (Fig. 2F), *Varanus exanthematicus* mPPt orientation is mostly dorsoventral (Fig. 2B) with less mediolateral component than *G. gecko*. *Psittacus erithacus* has a mostly mediolaterally oriented mPPt (Fig. 2E), and it is significantly more rostrocaudal than the mPPt orientations observed in *G. gecko*, *V. exanthematicus*, and *Tyrannosaurus rex* (Fig. 2C), which occupies similar mPPt orientation space as *V. exanthematicus* but is more mediolateral.

Comparisons of *m. levator pterygoideus* (mLPt) are limited to *G. gecko*, *V. exanthematicus*, and *T. rex* (Fig. 2A, B, C, G), as mLPt is lost in Aves (Holliday, 2009). Both lizards show remarkably dorsoventral mLPt orientation, with *V. exanthematicus* having a slightly rostrocaudal mLPt (Fig. 2B) and *G. gecko* (Fig. 2A) possessing a slightly mediolateral mLPt. In contrast, the mLPt in *T. rex* is almost completely mediolateral in orientation with a slight dorsoventral component (Fig. 2C).

Orientation space for *m. pterygoideus* (mPt; both *dorsalis* and *ventralis* muscle bellies; Fig. 2H, I) is less diverse than the *m. protractor pterygoideus* and *m. levator pterygoideus* muscle groups. *P. erithacus* possess the most dorsoventral mPtd (Fig. E), whereas *G. gecko* has the most rostrocaudal mPtd orientation (Fig. A). The orientation of mPt in *V. exanthematicus* (which lacks a ventralis belly; Holliday, 2009; Wilken *et al*., 2019) is markedly similar in orientation to mPtd in *G. gecko* (Fig. 2A). The mPtd of *P. erithacus* is oriented mildly dorsoventral (Fig. 2E). The mPtd of *G. gallus* occupies the center of this range of muscle orientations (Fig. 2D) and is almost equally rostrocaudal and dorsoventral in orientation to *P. erithacus*. Finally, *T. rex* has a mildly dorsoventral mPtd, similar to *G. gallus* and *P. erithacus*, although the mPtd in *T. rex* is slightly more mediolateral. The orientations for mPtv among *T. rex*, *G. gallus*, and *P. erithacus* are varying degrees of rostrocaudal (Fig. 2I). *Gallus gallus* and *T. rex* almost overlap in mPtv orientation and have mPtv muscle bellies that are mostly rostrocaudal with an appreciable mediolateral and dorsoventral component (Fig. 2C, D). *Psittacus erithacus* mPtv orientation is also mostly rostrocaudal (Fig. 2E), but with reduced dorsoventral and mediolateral components compared to *T. rex* and *G. gallus*. The orientation of mPtv in *G. gecko* is almost completely rostrocaudal, with a slight mediolateral component (Fig. 2A).

Pterygoid Shape and Bending Resistance

Bending is best resisted along the major axis whereas it is least resisted along the minor axis. In both squamates, the major axis is mediolateral and the minor axis is dorsoventral, although for much of the length of the pterygoid the magnitudes of both axes are fairly close (Fig. 3A, B). In *T. rex* the major axis is dorsoventral and the minor axis is mediolateral (Fig. 3C). The major axis for both birds is dorsoventral and their minor axis is mediolateral (Fig. 3D,E).

The lepidosaur pterygoids sampled here from *Gekko gecko* and *Varanus exanthematicus* are grossly similar in shape (Fig. 3A, B), being tube-shaped structures that flatten dorsoventrally in rostral sections as they bifurcate mediolaterally to connect to the palatine and maxilla, respectively. In contrast, the avian pterygoids sampled remain a consistent tube throughout their length (Fig. 3D,E). The pterygoid of *Tyrannosaurus rex* is remarkably different from the tubular construction of the

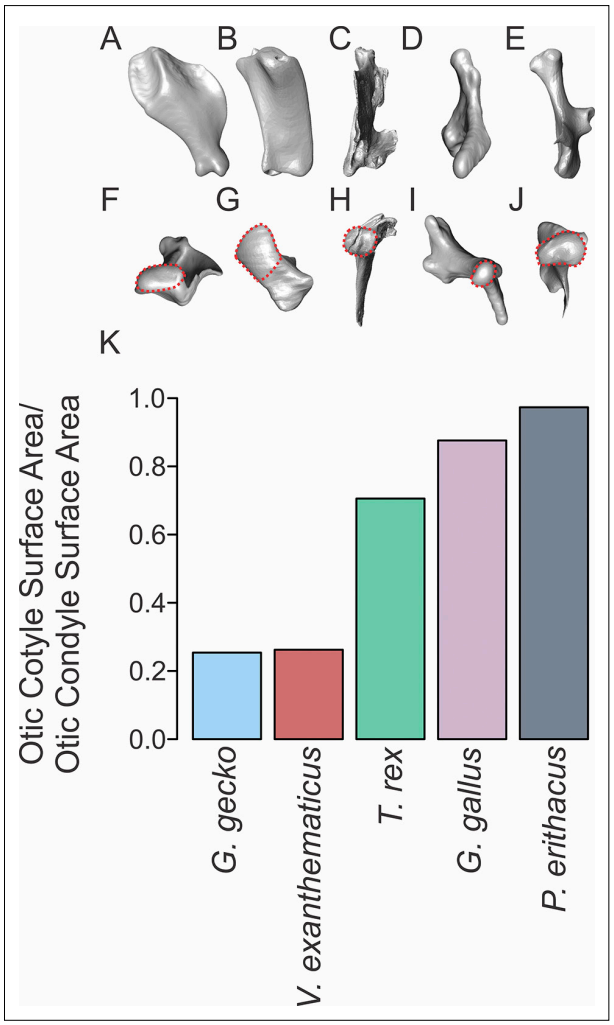

Fig. 4. Otic joint congruency. A, rostral view of left *Gekko gecko* quadrate, B, rostral view of left *Varanus exanthematicus* quadrate, C, rostral view of left *T. rex* quadrate, D, rostral view of left *Gallus gallus* quadrate, E, rostral view of left *Psittacus erithacus* quadrate, F, dorsal view of left *G. gecko* quadrate, G, dorsal view of left *V. exanthematicus* quadrate, H, dorsal view of left *T. rex* quadrate, I, dorsal view of left *G. gallus* quadrate, J, dorsal view of left *P. erithacus* quadrate, and K, otic joint congruency variation. The area inside the red, dotted lines represents hypothesized functional otic condyle area. The two squamates have dramatically larger otic condyles relative to their otic cotyles, as opposed to the dinosaurs, which have more congruent otic joints.

lizard and bird pterygoid. The rostral, palatine process of the pterygoid is mediolaterally compressed and narrow where it sutures to the palatine medially and ectopterygoid laterally. The caudal, quadrate process of the *T. rex* pterygoid is dorsoventrally tall and very thin mediolaterally (Fig. 3C). Only the narrow isthmus of the body of the pterygoid is tubular in shape and homogenous in cross section (BROCHU, 2003) near where it articulates with the robust basipterygoid process. This plate-like pterygoid is likely very weak against mediolateral bending and axial twisting. By calculating bending resistance, we were able to quantify and compare these aspects of pterygoid morphology across disparate sauropsid lineages.

Joint Surface Areas

The area of the quadrate articular surface was compared to the area of the squamosal articular surface. We found that the squamates maintain relatively larger quadrate surfaces, while the dinosaurs tend to have relatively smaller quadrate surfaces (Fig. 4). Birds especially show the relatively smallest quadrate surfaces in this study (Fig. 4).

Suspensoric Loading

To visualize the loading environments of the suspensorium in the taxa sampled here, we show von Mises equivalent deviatoric strain color maps (Fig. 5). *Gekko gecko* has large loads on its pterygoid in all directions, with its quadrate being primarily loaded in the dorsoventral (YY) direction (Fig. 5A). *Varanus exanthematicus* has large loads in the rostrocaudal (ZZ) and dorsoventral axes. The loads on its quadrate are mostly dorsoventrally oriented (Fig. 5B). Both squamates demonstrate considerable torsion in their pterygoids (Fig. 5A,B). *Tyrannosaurus rex* mostly loads it pterygoid in the dorsoventral axis, although there is considerable rostrocaudal loading as well (Fig. 5C). *Tyrannosaurus rex* loads its quadrate mainly in the rostrocaudal direction (Fig. 5C). *Gallus gallus* shows comparatively little loading on its pterygoid and quadrate, although its quadrate experiences some dorsoventral strains (Fig. 5D). *Psittacus erithacus* also demonstrates less suspensoric loading compared to either squamate or *T. rex*, but there is noticeable loading in the dorsoventral axis on both the pterygoid and quadrate of *P. erithacus* (Fig. 5E).

Otic Joint Loading

Principal strains demonstrate the loading environment of the joint articular surfaces (Fig. 6). The first principal strain represents the maximum tensile strain and the third principal strain represents the minimum compressive strain. It is important to note that our models operate under many assumptions that may affect the magnitude of strain, such as material properties (detailed in Table 1) and full muscle activation.

The two lizards experience most loading on the quadrate. *Varanus exanthematicus*, for example, has a mean $\mathfrak{E}_1$ of 7000 μ_ε and a mean $\mathfrak{E}_3$ of –7000 μ_ε (Fig. 6). *Gekko gecko* has a mean $\mathfrak{E}_1$ of 6000 μ_ε and a mean $\mathfrak{E}_3$ of –10000 μ_ε, implying *G. gecko* experiences a much wider range of loadings on the quadrate (Fig. 6). The birds show little to no loading on the quadrate articular surface with *Psittacus erthacus* having a mean $\mathfrak{E}_1$ of 1000 μ_ε and a mean $\mathfrak{E}_3$ of –1000 μ_ε and *Gallus gallus* having a mean of 0.000 μ_ε for all principal strains (Fig. 6). *Tyrannosaurus rex* experiences no compression on the quadrate, but experiences very mild tensile and shear loading. *T. rex* has a mean $\mathfrak{E}_1$ of 2000 μ_ε and a mean $\mathfrak{E}_3$ of –2000 μ_ε (Fig. 6). Further-

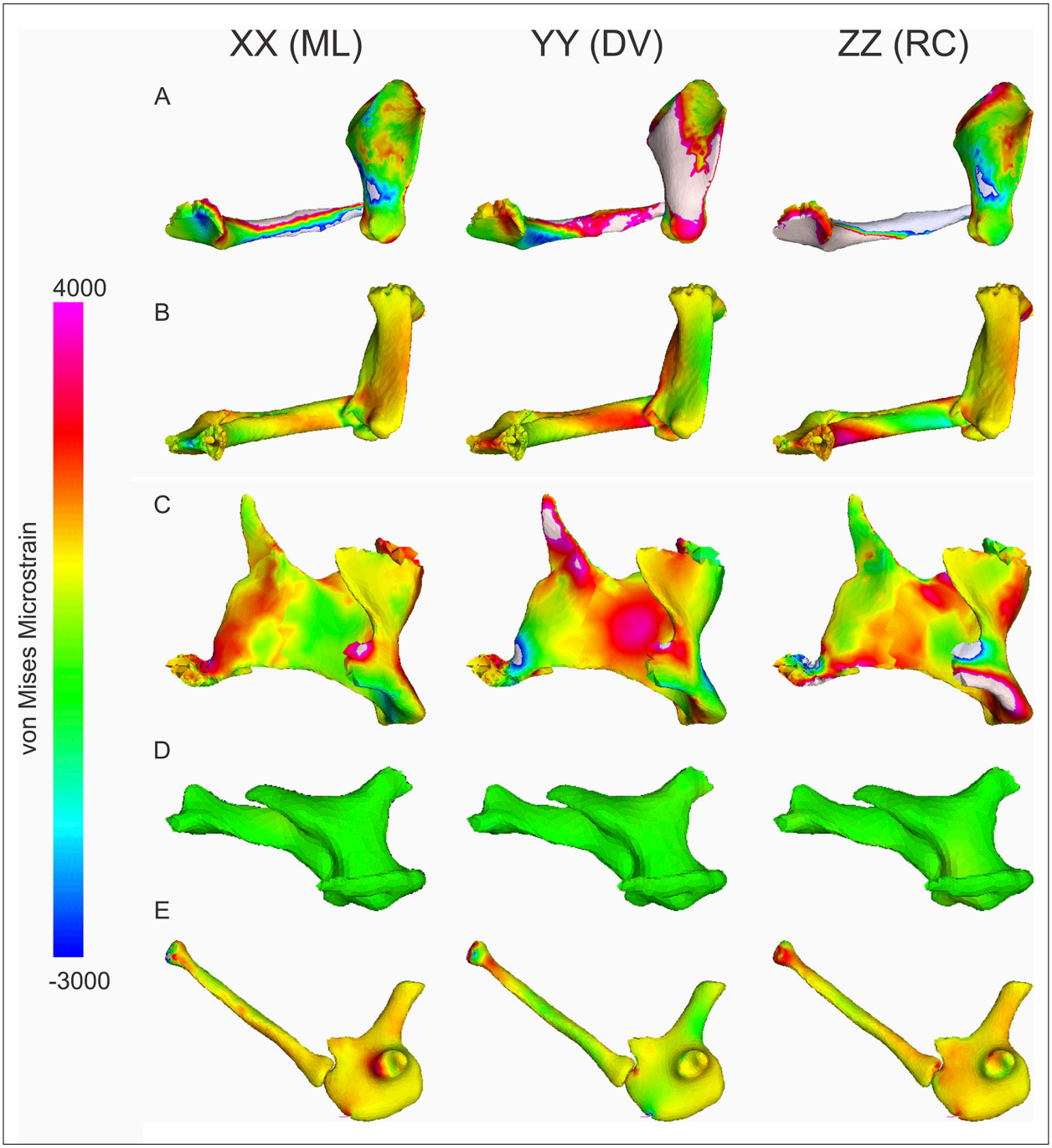

Fig. 5. Von Mises equivalent deviatoric microstrain in the suspensorium. A, *Gekko gecko*, B, *Varanus exanthematicus*, C, *Tyrannosaurus rex*, D, *Gallus gallus*, and E, *Psittacus erithacus*. Warmer colors represent tensile strains and cooler colors represent compressive strains. *T. rex* experiences little mediolateral (XX) loading on its suspensorium, in contrast with the two squamates and *P. erithacus*.

more, all animals demonstrated little variance in loading across the different aspects of the quadrate articular surface.

Discussion

This study illustrates new metrics of morphological and biomechanical diversity in the sauropsid skull and feeding apparatus. Our novel approaches enable disparate taxa to be characterized with respect to pterygoid bending properties, joint surface area, joint congruence, and muscle orientation and compared using the same quantitative criteria. We systematically characterize the differences in component structure and muscles arrangement. We also identify associated differences in loading and mechanical properties of the suspensorium. Although our sample is admittedly limited, these richly informative models provide a framework for deeper investigations into the functional and phylogenetic patterns underlying the evolution and development of the skull.

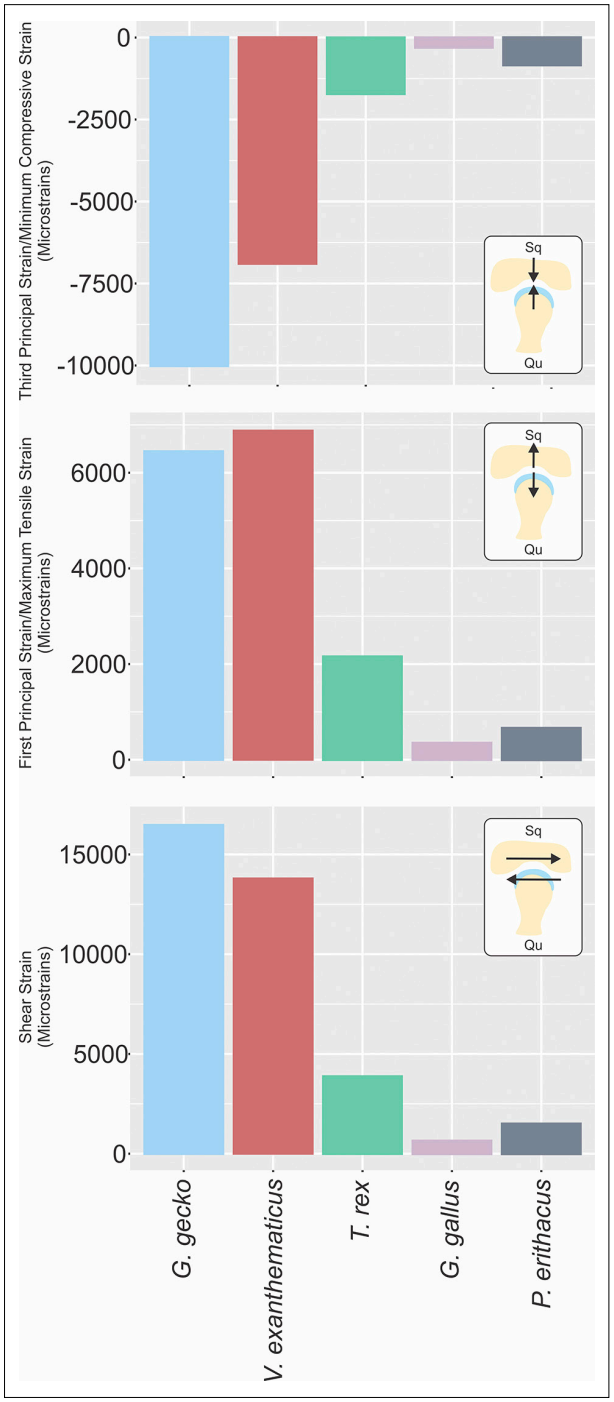

Fig. 6. Otic condyle loading in principal strains. The third principal strain represents the greatest compressive load, while the second principal strain represents the greatest tensile load. Shear strain is the differential of these two loads. The two squamates experience the greatest loading regimes on their otic condyle.

Squamates and archosaurs differ in the relative size of the quadrate otic condyle (Fig. 4), which may inform function and mechanical role. The quadrate is key to linking the neurocranium and mandible, and its shape is highly variable in shape in reptiles (HOLLIDAY & WITMER, 2008; HENDRICKX *et al.*, 2015; PALUH & BAUER, 2018; PALCI *et al.*, 2019). There is also great diversity in the morphology of the otic condyle of the quadrate (HENDRICKX *et al.*, 2015) that supports functional hypotheses for changes in morphology. Indeed, PALCI *et al.* (2019) found that a considerable amount of quadrate diversity in squamates can be attributed to ecology, phylogeny plays almost no role in quadrate diversity, and cranial biomechanics appear to be the primary driver of quadrate shape change in squamates. Mechanically, a larger otic condyle provides more surface area to distribute forces and may suggest more variation in the direction of loading. There are other biological factors that may explain the changes in quadrate morphology. The smaller otic condyle could be constrained by phylogenetic inertia endemic to archosaurs (or dinosaurs), as the neurocranial skeletal elements are described as well-integrated in archosaurs (FELICE *et al.*, 2019). There are also the questions of the effects of allometric scaling and paedomorphosis on the quadrate. It is also important to consider how much of the otic head of the quadrate is functionally the otic condyle. For example, *Varanus exanthematicus* has a large otic surface that may instead serve as attachment for ligamentous connections, similar to the antitrochanter fibrocartilage on the lateral surface of archosaurian ilio- and ischial peduncles (TSAI & HOLLIDAY, 2015).

Despite different loading environments (and perhaps linkage functions), the pterygoids of squamates and avian taxa both converge on tubular morphologies in the midshaft of the pterygoid (Fig. 7). Furthermore, both kinetic lineages evolved from akinetic taxa with thin, vertical, plate-like pterygoids (EVANS, 2008; HOLLIDAY & WITMER, 2008). Here loading (Fig. 5) matches pterygoid cross-sectional geometry (Figs 3,7). This could be due to modeling parameters and construction of our FEA models, namely full muscle activation and placement of constraints, or because the feeding apparatus is more constrained and predictable than the locomotor apparatus (GRANATOSKY *et al.*, 2019; OLSEN, 2019). These modeling parameters also make comparisons to differently constructed models difficult, although our models show relatively similar strain distributions as models of similar taxa (RAYFIELD, 2005; MORENO *et al.*, 2008; PARR *et al.*, 2012; MCCURRY *et al.*, 2015). Palatal cross-sectional geometry is a relatively untapped tool for explorations into evolution, ecology, and morphology. For example, the *T. rex* pterygoid is a thin, vertical plate like structure, which may act as a brace for the braincase. A similar role has been suggested to occur in plesiosaurs (TAYLOR, 1992). Thin, vertical palates such as this can handle large dorsoventral loads, but extreme loading in the mediolateral or rostrocaudal directions threaten to break the pterygoid. Furthermore, expansion of the dinosaur braincase likely reoriented jaw musculature from dorsoventral to rostrocaudal (HOLLIDAY, 2009; BHULLAR *et al.*, 2016) and presumably added greater mediolateral components to these jaw muscles as well. Reoriented jaw musculature in concert with other morphological changes may have resulted in the tubularization of the avian pterygoid.

Birds orient protractor muscles rostrocaudally, as opposed to squamates which maintain a dorsolateral protractor orientation (Fig. 2). The protractor musculature

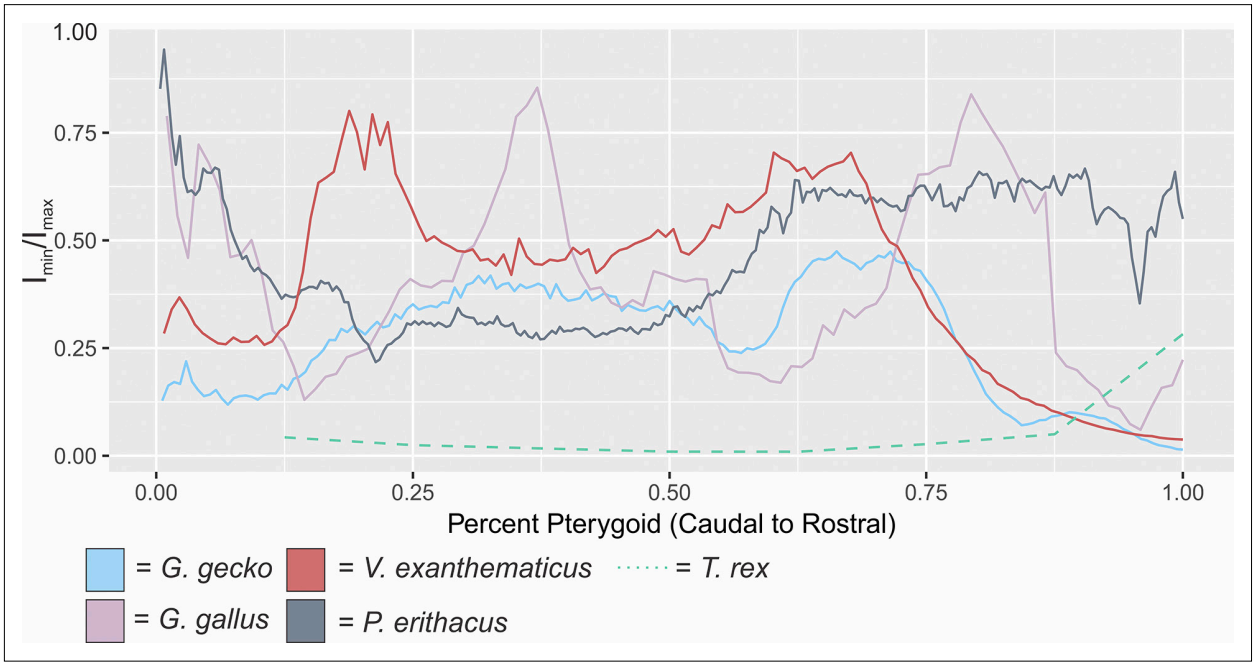

Fig. 7. Comparative pterygoid cross sectional geometries. Dividing I_{min} by I_{max} standardizes the bending resistance and data and illustrates ellipticity of the pterygoid. Values closer to 1.00 are rounder, while values closer to 0.00 are more oblong in shape. All the extant taxa samples converge on a tubular geometry in the midshaft of the pterygoid.

plays many roles in the sauropsid skull, such as powering prokinesis in birds (Bout & Zeigler, 1994; Claes *et al*., 2017) or mediating forces in the palate (Wilken *et al*., 2019), and elaboration of these muscles are key to kinesis in both squamates and birds. For example, birds have lost their *m*. *levator pterygoideus*, while snakes, the squamate lineage with the most accomplished cranial kinesis, gained novel protractor musculature, such as *m*. *retractor pterygoideus* and *m*. *protractor quadrati*, while reorienting their protractor rostrocaudally, similar to birds (Cundall, 1983). *Varanus exanthematicus*, *Gekko gecko*, and *Tyrannosaurus rex* all have dorsolaterally oriented protractor muscles, but varying degrees of kinetic ability (Metzger, 2002; Cost *et al*., 2019), suggesting neuromuscular modularity or other physiological control of protractor muscle function may influence cranial kinesis.

Integrating these morphological and biomechanical data reveals three morphotypes of pterygoid in this study: brace, propulsive, and torsional (Fig. 8). The brace pterygoid (e.g., *T. rex*) is mediolaterally thin and primarily loaded in the dorsoventral direction. Protractor muscles attaching to a brace pterygoid are dorsoventrally oriented. The propulsive pterygoid (e.g., *P. erithacus*) is tubular and loaded in the mediolateral and rostrocaudal axes. Propulsive pterygoids have rostrocaudally oriented protractor muscles and no *m*. *levator pterygoideus* attachment. Finally, the torsional pterygoid (e.g., *V. exanthematicus*) is tubular and experiences axial torsional loading. Despite the limited sample size, this pterygoid classification system provides a valuable glimpse into the evolution of the sauropsid suspensorium (Fig. 8).

This study highlights the diversity of form and functional complexity in the suspensorium of sauropsids. Elucidating and evaluating the broader patterns of diversity among loading, joint morphology, and cross-sectional geometry in the suspensorium requires further sampling across Sauropsida (Fig. 8).

Conclusions

Cranial joints are remnants of development (Iordansky, 1989; Brazeau & Ahlberg, 2006; Holliday & Witmer, 2008) that link the neurocranium to the suspensorium. Disparate lineages of sauropsids have co-opted these linkages into cranial kinesis. Animals with different modes of cranial kinesis vary in joint construction, muscle forces, and loading environment, demonstrating the diversity in the evolution of the neurocranium among diapsids. Here, we successfully compared and quantified a suite of traits related to the biomechanics of the suspensorium across a range of disparate sauropsids using a common criteria. We show that squamates likely place relatively larger loads on their otic joints than dinosaurs, have relatively larger otic condyles than dinosaurs, that birds and squamates both converge on tubular pterygoids, and that there may be a trend towards reorientation of protractor muscles in the evolution of birds. Our approaches provide a promising framework to further explore the function of the suspensorium and diversity of cranial kinesis.

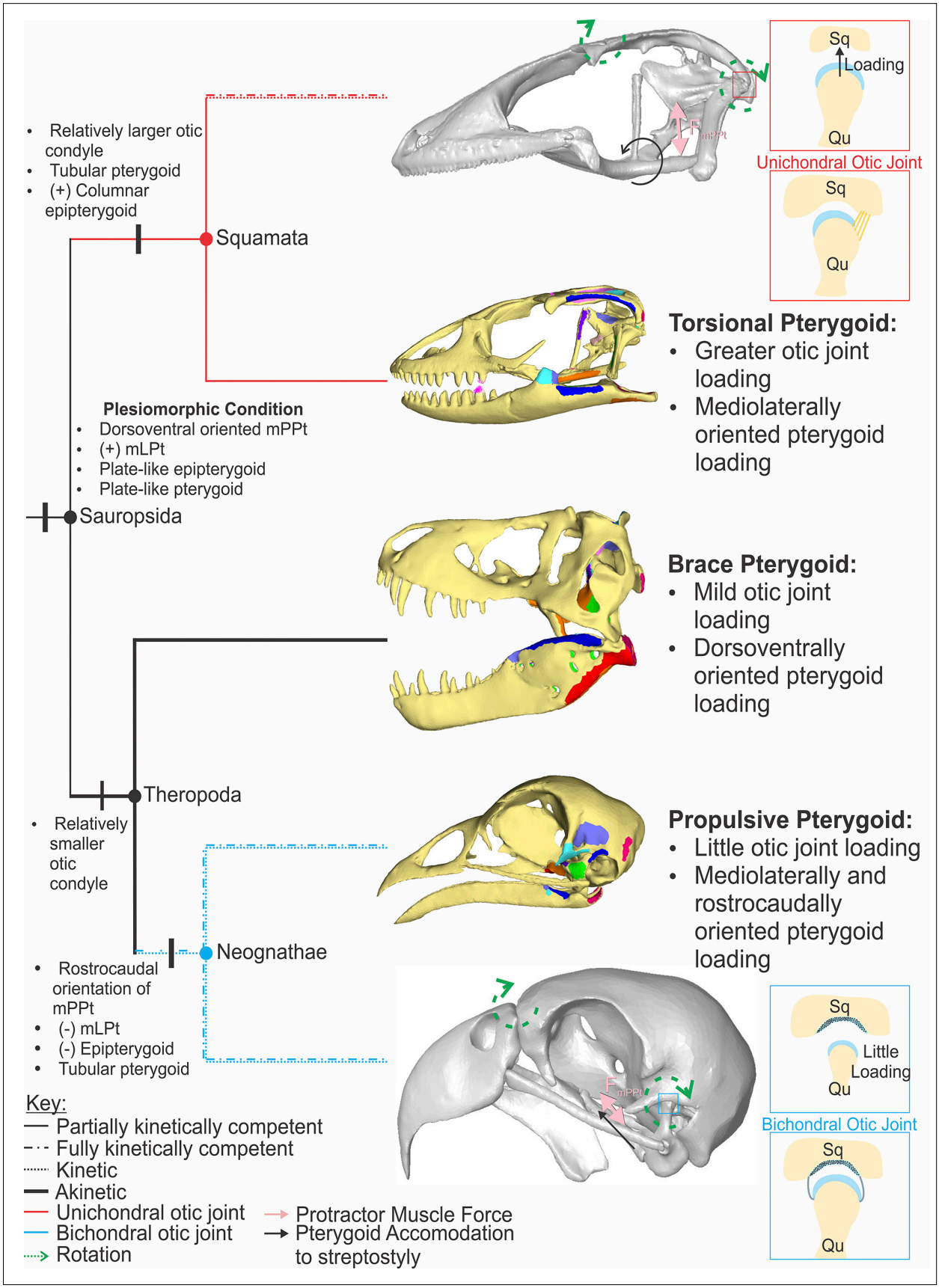

Fig. 8. Evolution and biomechanics of the sauropsid suspensorium. The suspensorium has diverse functions in the taxa sampled here and a complex evolutionary history. Different muscle loads, otic joint constructions, and pterygoid cross-sectional geometries result in biomechanically very different palates. Our proposed "brace pterygoid" is the plesiomorphic condition for sauropsids. Lineages possessing a brace pterygoid give rise to lineages with propulsive pterygoids and torsional pterygoids, as well as other palate morphotypes not studied here. **mLPt,** *m. levator pterygoideus;* **mPPt,** *m. protractor pterygoideus;* **Qu,** quadrate, **Sq,** squamosal.

Acknowledgments

We thank Lawrence Witmer, Alida Bailleul, Jul Davis, John Fortner, Aaron Olsen, and Marc Jones for insightful discussion, assistance, and advice as well as the reviewers whose comments further improved the paper. We thank Peter Larson at the Black Hills Institute and Art Anderson at Virtual Surface for permission to use the 3D model of BHI 3033. Finally, we thank Ingmar Werneburg for inviting us to submit this work as part of the symposium at the 2019 International Congress of Vertebrate Morphology. This study was funded by MU LSUROP, NSF REU grant IOS 1457319, NSF IOS 520100, and NSF 1457319.

References

Bailleul, A. M. & holliday, C. M. (2017). Joint histology in *Alligator mississippiensis* challenges the identification of synovial joints in fossil archosaurs and inferences of cranial kinesis. *Proceedings of the Royal Society B*, **284**, 20170038.

Bailleul, A. M., Witmer, L. M. & Holliday, C. M. (2017). Cranial joint histology in the mallard duck (*Anas platyrhynchos*): new insights on avian cranial kinesis. *Journal of Anatomy*, **230**, 444–460.

Bailleul, A. M. & Holliday, C. M. (2018). Retracing the evolution of the otic joint in birds and fossil theropods through histology: new insights into streptostyly, Abstract 116-1 *in*: *Annual Meeting of the Society of Integrative and Comparative Biology* (*SICB*). San Francisco, CA, SICB, http://www.sicb.org/meetings/2018/schedule/abstractdetails.php?id=127 (Accessed 8 June 2020)

Bellairs, A. d.'A. & Kamal, A.M. (1981). The chondrocranium and the development of the skull in recent reptiles, pp. 1–263, *in:* Gans, C. (ed.) *Biology of the Reptilia*. *Morphology F*, *Vol. 11*, London, Academic Press.

Beaupré, G., Stevens, S. & Carter, D. (2000). Mechanobiology in development, maintenance, and degeneration of articular cartilage. *Journal of Rehabilitation Research and Development*, **37**, 145–151.

Bhullar, B. S., Hanson, M., Fabbri, M., Pritchard, A., Bever, G. S. & Hoffman, E. (2016). How to make a bird skull: major transitions in the evolution of the avian cranium, paedomorphosis, and the beak as a surrogate hand. *Integrative and Comparative Biology*, **56**, 389–403.

Bout, R. G. & Zeigler, H. P. (1994). Jaw muscle (EMG) activity and amplitude and scaling of jaw movements during eating in pigeon (*Columba livia*). *Journal of Comparative Physiology A*, **174**, 433–442.

Bout, R. G. & Zweers, G. A. (2001). The role of cranial kinesis in birds. *Comparative Biochemistry and Physiology Part A Molecular and Integrative Physiology*, **131**, 197–205.

Brazeau, M. D. & Ahlberg, P. (2006). Tetrapod-like middle ear architecture in a Devonian fish. *Nature*, **439**, 318–321.

Brochu, C. A. (2003). Osteology of *Tyrannosaurus rex:* Insights from a nearly complete skeleton and high-resolution computed tomographic analysis of the skull. *Journal of Vertebrate Paleontology*, **22**, 1–138.

Cerny, R., Lwigale, P., Ericsson, R., Meulemans, D., Epperlein, H.H. & Bronner-Fraser, M. (2004). Developmental origins and evolution of jaws: new interpretations of "maxillary" and "mandibular". *Developmental Biology*, **276**, 225–236.

Claes, R., Muyshondt, P. G. G., Hoorebeke, L. V., Dhaene, J., Dirckx, J. J. J. & Aerts, P. (2017). The effect of craniokinesis on the middle ear of domestic chickens (*Gallus gallus domesticus*). *Journal of Anatomy*, **230**, 414–423.

Cost, I. N., Middleton, K. M., Sellers, K. C., Echols, M. S., Witmer, L. M., Davis, J. L. & Holliday, C. M. (2020). Palatal biomechanics and its significance for cranial kinesis in *Tyrannosaurus rex*. *The Anatomical Record*, **303**, 999–1017

Cundall, D. (1983). Activity of head muscles during feeding by snakes: a comparative study. *American Zoologist*, **23**, 383–396.

Curtis, N., Jones, M. E. H., Evans, S. E., O'Higgins, P. & Fagan, M. J. (2013). Cranial sutures work collectively to distribute strain throughout the reptile skull. *Journal of the Royal Society Interface*, **10**, 20130442.

Davis, J. L., Santana, S. E., Dumont, E. R. & Grosse, I. R. (2010). Predicting bite force in mammals: two-dimensional versus three-dimensional models. *Journal of Experimental Biology*, **213**, 1844–1851.

Dawson, M. M., Metzger, K. A., Baier, D. B. & Brainerd, E. L. (2011). Kinematics of the quadrate bone during feeding in mallard ducks. *Journal of Experimental Biology*, **214**, 2036–2046.

Doube, M., Klosowski M. M., Arganda-Carreras, I., Cordelieres, F., Dougherty, R. P., Jackson, J., Schmid, B., Hutchinson, J. R. & Shefelbine, S. J. (2010). BoneJ: free and extensible bone image analysis in ImageJ. *Bone*, **47**, 1076–9.

Evans, S. E. (2003). At the feet of the dinosaurs: the early history and radiation of lizards. *Biological Review*, **78**, 513–551.

Evans, S. E. (2008). The skull of lizards and tuatara, pp. 1-347 *in:* Gans, C., Gaunt, A. S. & Adler, K. (eds) *Biology of the Reptilia*, *Vol. 20*. New York, Society for the Study of Amphibians and Reptiles.

Frazzetta, T. (1962). A functional consideration of cranial kinesis in lizards. *Journal of Morpology*, **111**, 287–320.

Felice, R. N., Watanabe, A., Cuff, A. R., Noirault, E., Pol, D., Witmer, L. M., Norell, M. A., O'Connor, P. M. & Goswami, A. (2019). Evolutionary integration and modularity in the archosaur cranium. *Integrative and Comparative Biology*, **59**, 371–382.

Gardner, N. M., Holliday, C. M. & O'Keefe, F. R. (2010). The braincase of *Youngina capensis* (Reptilia, Diapsida): new insights from high-resolution CT scanning of the holotype. *Palaeontologia Electronica*, **13**, 16 pp.

Gans, C. (1982). Fiber architecture and muscle function. *Exercise and Sports Science Review*, **10**, 160–207.

Gignac, P. M., Kley, N. J., Clarke, J. A., Colbert, M. W., Morhardt, A. C., Cerio, D., Cost, I. N., Cox, P. G., Daza, J. D., Early, C. M., Echols, M. S., Henkelman, R. M., Herdina, A. N., Holliday, C. M., Li, Z,. Mahlow, K., Merchant, S., Müller, J., Orsbon, C. P., Paluh, D. J., Thies, M. L., Tsai, H. P. & Witmer, L. M. (2016). Diffusible iodine-based contrast-enhanced computed tomography (diceCT): an emerging tool for rapid, high-resolution, 3-D imaging of metazoan soft tissues. *Journal of Anatomy*, **228**, 889–909.

Granatosky, M. C., McElroy, E. J., Laird, M. F., Iriarte-Diaz, J., Reilly, S. M., Taylor, A. B. & Ross, C. F. (2019). Joint angular excursions during cyclical behaviors differ between tetrapod feeding and locomotor systems. *Journal of Experimental Biology*, **222**, jeb200451.

Gussekloo, S. W., Vosselman, M. G. & Bout, R. G. (2001). Three-dimensional kinematics of skeletal elements in avian prokinetic and rhynchokinetic skulls determined by Roentgen stereophotogrammetry. *Journal of Experimental Biology*, **204**, 1735–1744.

Hall, B. K. (2005). *Bones and Cartilage: Developmental and Evolutionary Skeletal Biology*. San Diego, *Elsevier Academic Press*.

Hanken, J. & Hall, B. K. (Eds., 1993). *The Skull*, *Volume 2: Patterns of Structural and Systemic Diversity*. Chicago, University of Chicago Press.

Haut, R. C., Lancaster, R. L. & DeCamp, C. E. (1992). Mechanical properties of the canine patellar tendon: some correlations with age and the content of collagen. *Journal of Biomechanics*, **25**, 163–173.

Hendrickx, C., Araújo, R. & Mateus, O. (2015). The non-avian theropod quadrate I: standardized terminology with an overview of anatomy and function. *PeerJ*3:e1245.

Herrel, A., Cleuren, J. & De Vree, F. (2000). Cranial kinesis in geckoes: functional implications. *Journal of Experimental Biology*, **203**, 1415–1423.

HIRASAWA, T. & KURATANI, S. (2015). Evolution of the vertebrate skeleton: morphology, embryology, and development. *Zoological Letters*, **1**, **2**.

HOLLIDAY, C. M. & WITMER, L. M. (2007). Archosaur adductor chamber evolution: integration of musculoskeletal and topological criteria in jaw muscle homology. *Journal of Morphology*, **268**, 457–484.

HOLLIDAY, C. M. & WITMER, L. M. (2008). Cranial kinesis in dinosaurs: intracranial joints, protractor muscles, and their significance for cranial evolution and function in diapsids. *Journal of Vertebrate Paleontology*, **28**, 1073–1088.

HOLLIDAY, C. M. (2009). New insights into dinosaur jaw muscle anatomy. *The Anatomical Record*, **292**, 1246–1265.

HOLLIDAY, C. M., TSAI, H. P., SKILJAN, R. J., GEORGE, I. D. & PATHAN, S. (2013). A 3D interactive model and atlas of the jaw musculature of *Alligator mississippiensis*. *PLOS One*, **8**, e62806.

IORDANSKY, N. N. (1989). Evolution of cranial kinesis in lower tetrapods. *Netherlands Journal of Zoology*, **40**, 32–54.

JONES, M. E., GRONING, F., DUTEL, H., SHARP, A., FAGAN, M. J. & EVANS, S. E. (2017). The biomechanical role of the chondrocranium and sutures in a lizard cranium. *Journal of the Royal Society Interface*, **14**, 20170637.

MCCURRY, M. R., MAHONEY, M., CLAUSEN, P. D., QUAYLE, M. R., WALMSLEY, C. W., JESSOP, T. S., WROE, S., RICHARDS, H. & MC HENRY, C. R. (2015). The relationship between cranial structure, biomechanical performance and ecological diversity in varanoid lizards. *PLoS ONE*, **10**, e0130625.

MCLAUGHLIN, E., ZHANG, Y., PASHLEY, D., BORKE, J. & YU, J. (2000). The load-displacement characteristics of neonatal rat cranial sutures. *Cleft Palate Craniofacial Journal*, **37**, 590–595.

METZGER, K. (2002). Cranial kinesis in lepidosaurs: skulls in motion, pp. 15–46 *in:* AERTS, P., D'AOÛT, K., HERREL, A. & VAN DAMME, R. (eds) *Topics in Functional and Ecological Vertebrate Morphology*. Düren, Shaker Publishing.

MEZZASALMA, M., MAIO, N. & GUARINO, F. M. (2014). To move or not to move: cranial joints in european gekkotans and lacertids, an osteological and histological perspective. *The Anatomical Record*, **297**, 463–472.

MOAZEN, M., CURTIS, N., O'HIGGINS, P., EVANS, S. E. & FAGAN, M. J. (2009a). Biomechanical assessment of evolutionary changes in the lepidosaurian skull. *PNAS*, **106**, 8273–8277.

MOAZEN, M., CURTIS, N., O'HIGGINS, P., JONES, M. E. H., EVANS, S. E. & FAGAN, M. J. (2009b). Assessment of the role of sutures in a lizard skull: a computer modelling study. *Proceedings of the Royal Society B*, **276**, 39–46.

MONTUELLE, S. J. & WILLIAMS, S. H. (2015). *In Vivo* measurement of mesokinesis in *Gekko gecko*: the role of cranial kinesis during gape display, feeding and biting. *PLoS One*, **10**, e0134710.

MORENO, K., WROE, S., CLAUSEN, P., MCHENRY, C., D'AMORE, D. C., RAYFIELD, E. J. & CUNNINGHAM, E. (2008). Cranial performance in the Komodo dragon (*Varanus komodoensis*) as revealed by high resolution 3-D finite element analysis. *Journal of Anatomy*, **212,** 736–746.

OLSEN, A. M. & WESTNEAT, M. W. (2016). Linkage mechanisms in the vertebrate skull: structure and function of three-dimensional, parallel transmission systems. *Journal of Morphology*, **277**, 1570–1583.

OLSEN, A. M. (2019). A mobility based classification of closed kinematic chains in biomechanics and implication for motor control. *Journal of Experimental Biology*, **222**, jeb195735.

PALCI, A., CALDWELL, M. W., HUTCHINSON, M. N., KONISHI, T. & LEE, M. S. Y. (2019). The morphological diversity of the quadrate bone in squamate reptiles as revealed by high-resolution computed tomography and geometric morphometrics. *The Anatomical Record*, **236**, 210–227.

PALUH, D. J. & BAUER, A. M. (2018). Phylogenetic history, allometry and disparate functional pressures influence the morphological diversification of the gekkotan quadrate, a keystone cranial element. *Biological Journal of the Linnean Society*, **125**, 693–708.

PARR, W. C. H., WROE, S., CHAMOLI, U., RICHARDS, H. S., MCCURRY, M. R., CLAUSEN, P. D., & MCHENRY, C. (2012). Toward integration of geometric morphometrics and computational biomechanics: new methods for 3D virtual reconstruction and quantitative analysis of Finite Element Models. *Journal of Theoretical Biology*, **301**, 1–14.

PAYNE, S. L., HOLLIDAY, C. M., VICKARYOUS, M. K. (2011). An osteological and histological investigation of cranial joints in geckos. *The Anatomical Record*, **294**, 399–405.

PEARSON, O. M. & LIEBERMAN, D. E. (2004). The aging of Wolff's "law": ontogeny and responses to mechanical loading in cortical bone. *Yearbook of Physical Anthropology*, **47**, 63-99.

RAYFIELD, E. J. (2005). Aspects of comparative cranial mechanics in the theropod dinosaurs *Coelophysis*, *Allosaurus*, and *Tyrannosaurus*. *Zoological Journal of the Linnean Society*, **144**, 309–316.

RAYFIELD, E. J. (2011). Strain in the ostrich mandible during simulated pecking and validation of specimen-specific finite element analysis. *Journal of Anatomy*, **218**, 59–74.

RIEPPEL, O. (1978). Streptostyly and muscle function in lizards. *Experientia*, **34,** 776–777.

RUFF, C., HOLT, B. & TRINKHAUS, E. (2006). Who's afraid of the big bad Wolff? "Wolff's Law" and bone functional adaptation. *American Journal of Physical Anthropology*, **129**, 484–498.

SACKS, R. D. & ROY, R. R. (1982). Architecture of the hind limb muscles of cats: functional significance. *Journal of Morphology*, **173**, 185–195.

SCHILLING, T. F. & THOROGOOD, P. V. (2000). Development and evolution of the vertebrate skull. *Linnean Society Symposium Series*, **20**, 57–84.

SCHNEIDER, C. A., RASBAND, W. S. & ELICEIRI, K. W. (2012). NIH Image to ImageJ: 25 years of image analysis. *Nature Methods*, **9**, 671–675.

SELLERS, K. C., MIDDLETON, K. M., DAVIS, J. L. & HOLLIDAY, C. M. (2017). Ontogeny of bite force in a validated biomechanical model of the American alligator. *Journal of Experimental Biology*, **220**, 2036–2046.

SMITH, K. K. (1980). Mechanical significance of streptostyly in lizards. *Nature*, **283**, 778–779.

STRAIT, D. S., WANG, Q., DECHOW, P. C., ROSS, C. F., RICHMOND, B. G., SPENCER, M. A. & PATEL, B. A. (2005). Modeling elastic properties in finite-element analysis: How much precision is needed to produce an accurate model? *The Anatomical Record*, **283A**, 275–287.

TAYLOR, M. A. (1992). Functional anatomy of the head of the large aquatic predator *Rhomaleosaurus zetlandicus* (Plesiosauria, Reptilia) from the Toarcian (Lower Jurassic) of Yorkshire, England. *Philosophical Transactions of the Royal Society of London*, *Series B*, *Biological Sciences*, **335**, 247–280.

TSAI, H. P. & HOLLIDAY, C. M. (2015). Articular soft tissue anatomy of the archosaur hip joint: structural homology and functional implications. *Journal of Morphology*, **276**, 601–630.

WERNEBURG, I. & MAIER, W. (2019). Diverging development of akinetic skulls in cryptodire and pleurodire turtles: an ontogenetic and phylogenetic study. *Vertebrate Zoology*, **69**, 113–143.

WILKEN, A. T., MIDDLETON, K. M., SELLERS, K. C., COST, I. N. & HOLLIDAY, C. M. (2019). The roles of joint tissues and jaw muscles in palatal biomechanics of the Savannah monitor (*Varanus exanthematicus*) and their significance for cranial kinesis. *Journal of Experimental Biology*, **222**, jeb201459.

VOGEL, S. (1988). *Life's Devices: The Physical World of Animals and Plants*. Princeton, NJ, Princeton University Press.

ZAPATA, U., METZGER, K., WANG, Q., ELSEY, R. M., ROSS, C. F. & DECHOW, P. C. (2010). Material properties of mandibular cortical bone in the American alligator, *Alligator mississippiensis*. *Bone*, **46**, 860–867.